Multielectron dynamics in the tunneling ionization of correlated quantum systems

Maximilian Hollstein and Daniela Pfannkuche
Universität Hamburg, I. Institut für Theoretische Physik, Jungiusstraße 9, 20355 Hamburg, Germany
(Received 12 June 2015; published 20 November 2015)

The importance of multielectron dynamics during the tunneling ionization of a correlated quantum system is investigated. By comparison of the solution of the time-dependent Schrödinger equation with the time-dependent configuration-interaction singles approach, we demonstrate the importance of a multielectron description of the tunneling ionization process especially for weakly confined quantum systems. Within this context, we observe that adiabatic driving by an intense light field can even enhance the correlations between still trapped electrons.

DOI: 10.1103/PhysRevA.92.053421 PACS number(s): 32.80.Fb, 32.80.Rm, 33.80.Rv

I. INTRODUCTION

The ionization of closed-shell atoms is impressively well understood on the basis of single active electron (SAE) approaches [1–3] or effective one-particle theories as the time-dependent configuration-interaction singles (TDCIS) approach [4–6]. Within these approaches, ionization is described by the ejection of a single electron into the continuum while the residual electrons remain unaffected; i.e., they are only taken into account by a time-independent potential for the active electron (SAE) or they are kept residing in Hartree-Fock ground-state orbitals of the field-free atom (TDCIS). However, in weakly confined quantum systems such as molecules or atomlike systems as semiconductor quantum dots in which the electron-electron interaction induces significant correlations between the trapped electrons [7–11], an independent particle description of the ionization process, as inherent in these approaches, is expectably unsuitable from the very beginning. In this paper, we address the question concerning the importance of a multielectron description of the tunneling ionization process of weakly confined and correlated quantum systems. For this purpose, we consider the dynamics which is induced by an intense low-frequency light field in a two-electron model system. Our conclusions drawn from these considerations, however, are not only valid for two-electron quantum systems but they are transferable to systems with more than two weakly bound electrons. Furthermore, we would like to remark that the conclusions drawn from the presented model calculations are not limited to the ionization of molecular or atomic systems but they are also relevant for experiments based on the application of a (time-dependent) voltage to semiconductor quantum dots [12,13] and photoassisted tunneling [12,14–17] in the low-frequency regime. This paper is structured as follows: after introducing the considered model system, we demonstrate the need for a multielectron description of the tunneling ionization process by comparison of the solution of the time-dependent Schrödinger equation (TDSE) with the results obtained by the TDCIS approach. By detailed analysis of the exact wave function we provide insight into the light-induced dynamics, revealing that a multielectron description becomes necessary not only due to ground-state correlations but also due to a light-induced collective electron motion which is accompanied with an enhancement of correlations between still trapped electrons.

II. MODEL

In order to study the ionization of a weakly confined quantum system, we consider a one-dimensional model system consisting of two electrons in an inverse Gaussian confining potential. (Note that the effective potential realized in semiconductor quantum dots can be well approximated by this potential [18,19]).

Referring to the spatial coordinate as x, the considered confining potential can be denoted by

$$V(x) = -V_0 e^{-(\frac{x}{w})^2} \tag{1}$$

where V_0 determines the depth and w determines the width of the confinement. Without exception, effective atomic units (see the Appendix) are used throughout this paper. For atoms and molecules, the chosen unit system coincides with the well-known atomic units. However, for GaAs quantum dots, for example, an effective Hartree is on the order of $\approx$11.86 meV and an intensity of 1.0 corresponds there to only $\approx 1.95 \times 10^5$ W/cm^2 [19,20]. Within the harmonic approximation of the considered potential, the strength of the confinement, i.e., the level spacing of the lowest bound states, is given by

$$\Delta E \approx \frac{\sqrt{2V_0}}{w}. \tag{2}$$

In the subsequent considerations we make use of this dependency and vary the strength of the confinement by variation of the width w.

The electron-electron interaction is taken into account by a regularized Coulomb interaction:

$$V_{ee}(x_1,x_2) = \frac{1}{\sqrt{(x_1 - x_2)^2 + \delta^2}} \tag{3}$$

where $x_{1,2}$ denote the spatial coordinates of the two electrons. By choosing δ unequal to zero (we set δ to 0.5), a finite width of the electronic wave function along the unconsidered spatial dimensions is taken into account in a phenomenological way [21,22]. Hereinafter, we restrict our considerations to light fields with a wavelength which is large compared to the extend of the considered quantum system. This allows the application of the dipole approximation to the light-matter interaction. Thus, in length gauge, the Hamiltonian of the quantum system

interacting with the light field is given by

$$\hat{H}_0 = -\frac{1}{2}\sum_{i=1}^{2}\frac{\partial^2}{\partial x_i^2} - V_0\sum_{i=1}^{2}e^{-(\frac{x_i}{w})^2} + \frac{1}{\sqrt{(x_1-x_2)^2+\delta^2}}, \quad (4)$$

$$\hat{H}(t) = \hat{H}_0 - \sum_{i=1}^{2} x_i E(t) \quad (5)$$

where $\hat{H}_0$ is the Hamiltonian of the field-free system and $E(t)$ denotes the time-dependent electric field of the laser. Subsequently, we consider the initial dynamics of the system in an electric field with sinusoidal time dependence, i.e.,

$$E(t) = E_0 \sin(\omega t). \quad (6)$$

In the following, we consider the situation where the two-electron system is initially prepared in the singlet ground state. In order to study the light-induced dynamics, we solve the time-dependent Schrödinger equation numerically. For this, we employ a split operator technique [23]. Here, we are only interested in the two-electron dynamics involved in the ionization process. That is, we are interested in the part of the wave function describing both electrons residing in the potential well or its vicinity. In this situation, a convenient numerical technique is the use of complex absorbing potentials or the (smooth) exterior scaling transformation [24,25]. There, a finite simulation box is employed to represent the wave function in the spatial region of interest and outgoing wave packets leaving the region are effectively damped when having spatial overlap with the complex absorbing potential or the region where the spatial coordinate is transformed. Therefore, these techniques prevent artificial reflections at the boundaries and allow the use of rather small simulation boxes that are only slightly larger than the region of interest. In the considered situation, their use allows for a significant reduction of computation time while still leading to converged results. In practice, we employed the complex absorbing potential V_{CAP}:

$$V_{\mathrm{CAP}} = \begin{cases} -iC(||x| - x_0|)^3 & |x| > x_0 \\ 0 & \text{else} \end{cases}. \quad (7)$$

For the calculations presented below, C is chosen to be 4×10^{-3}. x_0 is chosen to be 15 where both the confining potential and the ground-state wave function are only insignificant when different from zero (i.e., for all model parameters, the absolute value of the confining potential is for $x = 15$ smaller than 0.001 and the value of the ground-state density is decreased to $\lesssim 10^{-16}$). In this paper, we consider the tunneling ionization process, i.e., the ionization via tunneling through the effective potential barrier which is exhibited by the instantaneous potential $V(t)$ that is formed by the instantaneous electric field and the confining potential:

$$V(t) = -V_0 e^{-(\frac{x}{w})^2} - E(t)x. \quad (8)$$

For $|E| \geqslant E_{\mathrm{crit}}$ with

$$E_{\mathrm{crit}} = \frac{V_0}{w}\sqrt{\frac{2}{e}} \quad (9)$$

the instantaneous potential $V(t)$ does not possess a minimum so that E_{crit} marks the regime of a light-matter interaction that is dominant with respect to the confinement. Here, we focus on the regime where E_0 is comparable to E_{crit} but smaller so that the instantaneous potential is strongly deformed but still exhibits a potential barrier, i.e., $E_0/E_{\mathrm{crit}} \lesssim 1$. This regime depends strongly on the confinement, i.e., the depth and, in particular, the width. For instance, the considered regime can be reached by laser intensities lower than $\sim 10^{14}$ W/cm^2 for a quantum system with a confinement depth of $\sim$15 eV and a width of $\sim$10 a.u. Thus, our findings presented in this paper can be particularly relevant for strong-field ionization of polyatomic molecules. However, our results are also applicable to semiconductor quantum dots. For instance, for typical GaAs quantum dots [19] with a confinement depth on the order of 100 meV, the considered regime can be reached easily with intensities even lower than $\sim 1 \times 10^6$ W/cm^2. However, in the presented model calculations, we consider the described regime by setting $V_0 = 3$ and $E_0 = 0.3$ so that $E_0/E_{\mathrm{crit}} \lesssim 1$ for all considered confinement widths w ($1 \leqslant w \leqslant 5$).

Considering that the tunneling ionization regime is characterized by a Keldysh parameter [26] much smaller than 1, we choose the frequency of the light field to be $\omega = 2\pi \times 0.001$ and the amplitude to be $E_0 = 0.3$ corresponding to a Keldysh parameter smaller than 0.01 for the considered model potential parameters. For semiconductor quantum dots, the characteristic confinement energy is in the meV range so that the considered light field would be in the domain of far infrared light to microwaves. Since for tunneling ionization the ionization process is most prominent at times when the electric field of the light field is extremal, we consider only the dynamics during a half cycle of the laser field focusing on the situation at $t = T/4$ when the electric field is maximum. Here, we restrict our considerations to the dynamics in the confining potential well and its vicinity by analyzing the restricted and renormalized wave function

$$\tilde{\Psi} = \frac{\Psi(x_1,x_2,t)|_{|x_{1,2}|<x_{\max}}}{\sqrt{\int_{-x_{\max}}^{x_{\max}}\int_{-x_{\max}}^{x_{\max}} dx_1 dx_2 |\Psi(x_1,x_2,t)|^2}} \quad (10)$$

whereas, unless noted differently, we chose

$$x_{\max} = x_0 = 15. \quad (11)$$

Before the two-electron system is exposed to the light field, both electrons are situated in this area. However, at later times, electrons are excited by the laser into the continuum and leave the considered spatial region. During the considered half cycle, electrons that are tunneled through the potential barrier are only accelerated away from the confining potential minimum. This is reflected in the time-dependent norm of $\Psi(x_1,x_2,t)|_{|x_{1,2}|<x_{\max}}$, which decreases monotonically (see Fig. 1).

Noteworthy, this time-dependent norm becomes stationary even before the end of the considered half cycle, indicating that the electrons which tunneled through the potential barrier left the considered spatial region before the end of the half cycle. After the half cycle at $t = T/2$, the part of the wave function consisting of occupied continuum states has only an insignificant spatial overlap with the considered spatial region; more precisely, at $T/2$, the renormalized restricted wave function has for the considered parameters an overlap larger than 0.999 with the field-free ground state. For this reason, we determine numerically the ionization probability

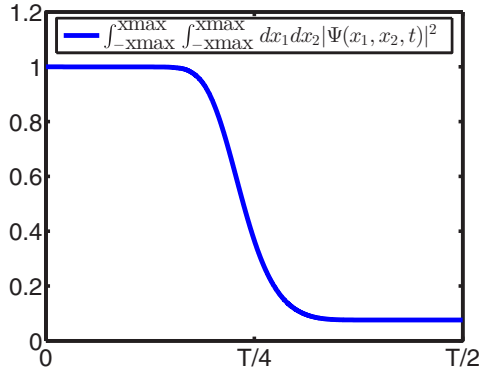

FIG. 1. (Color online) The time-dependent norm of $\Psi(x_1,x_2,t)|_{|x_{1,2}|<x_{\max}}$ during the first half cycle of the laser field for a confinement potential V [Eq. (1)] with $w = 5$. Here, $T = \frac{2\pi}{\omega}$ denotes the period of the considered light field and ω is the frequency of the light field [see Eq. (6)].

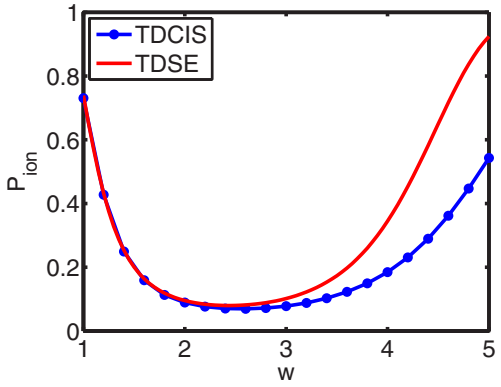

FIG. 2. (Color online) The ionization probability P_{ion} as defined in Eq. (12) after a half cycle of the laser field obtained by the solution of the TDSE (red curve) and by the TDCIS approach (blue curve with dots) in dependence on the width of the confinement w. All quantities in this figure are given in effective atomic units (see the Appendix). For narrow confinements (i.e., for $w < 2.5$), the TDCIS approach reproduces very accurately the exact ionization probability, whereas for wide confinements substantial deviations are observable.

conveniently by

$$P_{\text{ion}}(t) = 1 - \int_{-x_{\max}}^{x_{\max}} \int_{-x_{\max}}^{x_{\max}} dx_1 dx_2 |\Psi(x_1,x_2,t)|^2. \quad (12)$$

III. RESULTS

A. Comparison of TDCIS and TDSE

Within the TDCIS approach, the two-electron wave function is expanded in the Hartree-Fock ground state $|\Phi_0\rangle$ and its particle-hole excitations $|\Phi_0^i\rangle$:

$$|\Psi\rangle = \alpha_0 |\Phi_0\rangle + \sum_{i>0} \alpha_0^i |\Phi_0^i\rangle \quad (13)$$

with

$$|\Phi_0^i\rangle = \tfrac{1}{\sqrt{2}}(c_{i\uparrow}^\dagger c_{0\uparrow} + c_{i\downarrow}^\dagger c_{0\downarrow})|\Phi_0\rangle \quad (14)$$

where $c_{0\uparrow}, c_{0\downarrow}$ denote annihilation operators of the spin orbitals which are occupied in the Hartree-Fock ground-state determinant while $c_{i\uparrow}^\dagger, c_{i\downarrow}^\dagger$ denote creation operators of virtual orbitals. The spatial part of the TDCIS singlet two-electron wave function is consequently given by

$$\Psi(x_1,x_2,t)_{\text{TDCIS}} = \sum_i \tilde{\alpha}_i(t)\big[\psi_0(x_1)\psi_i(x_2) + \psi_i(x_1)\psi_0(x_2)\big] \quad (15)$$

with

$$\tilde{\alpha}_i(t) = \begin{cases} \alpha_0(t)/2 & i = 0 \\ \alpha_0^i(t) & \text{else} \end{cases}. \quad (16)$$

As can be seen in Eq. (15), at all times, only one electron can be active (i.e., occupy an arbitrary orbital) while the other electron is forced to occupy the Hartree-Fock ground-state orbital ψ_0.

In order to determine the coefficients $\tilde{\alpha}_i(t)$ we solve the Hartree-Fock equations on a pseudospectral grid as described in [25]. The TDCIS wave function is then propagated by iterative Lanczos reduction [27] within the configuration-interaction singles singlet subspace constructed by the eigenfunctions of the Fock operator. In Fig. 2, the ionization probability as defined in Eq. (12) obtained by the exact solution of the TDSE and by the TDCIS approach is shown for varying confinement widths. As can be seen, the TDCIS approach reproduces very accurately the exact ionization probability for $w < 2.5$ whereas large deviations are observable for $w > 2.5$ (e.g., by 40% for $w = 5$).

Some insight can be gained by the approximation of the exact two-electron wave function in terms of configurations constructed from the two most occupied natural orbitals [see Eq. (17)]. This truncated configuration-interaction expansion allows a good approximation of the exact wave function since the natural orbitals constitute an orbital basis set leading to the most rapidly converging expansion in configurations [28]:

$$\Psi \approx \sum_{i,j=1}^{2} c_{ij}\phi_i(x_1)\phi_j(x_2) \Big/ \sqrt{\sum_{i,j=1}^{2} |c_{ij}|^2}. \quad (17)$$

If the coefficients c_{ij} are real, this approximate wave function can be represented exactly in open-shell form [29] where one electron occupies a spatial orbital ϕ_u while the other electron occupies a different orbital ϕ_v, which is not necessarily completely orthogonal or totally parallel to ϕ_u:

$$\Psi(x_1,x_2,t) \approx \phi_u(x_1,t)\phi_v(x_2,t) + \phi_v(x_1,t)\phi_u(x_2,t). \quad (18)$$

Although the coefficients c_{ij} of the approximate wave function (17) obtained from the numerical propagation are complex at $t = T/4$, we found for this situation that with good accuracy c_{00} and c_{11} can be chosen real with alternating sign. Since c_{01} and c_{10} vanish exactly [30,31], a representation in open-shell form is nonetheless possible. As described in [29], ϕ_u and ϕ_v can be chosen as

$$\phi_u = \big(|c_{00}|^{\frac{1}{2}}\phi_0 + |c_{11}|^{\frac{1}{2}}\phi_1\big)/[4(|c_{00}|^2 + |c_{11}|^2)]^{\frac{1}{4}}, \quad (19)$$

$$\phi_v = \big(|c_{00}|^{\frac{1}{2}}\phi_0 - |c_{11}|^{\frac{1}{2}}\phi_1\big)/[4(|c_{00}|^2 + |c_{11}|^2)]^{\frac{1}{4}}. \quad (20)$$

With this, for instance for $w = 5$, both wave functions [Eqs. (17) and (18)] have an overlap of 0.967 with the exact wave function and thus provide a reasonable approximation.

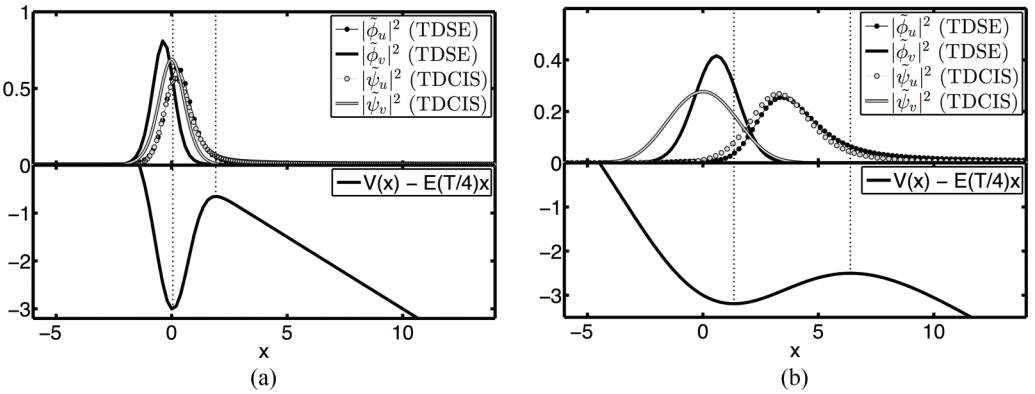

FIG. 3. The renormalized orbitals $\tilde{\phi}_{u,v} = \frac{\phi_{u,v}}{||\phi_{u,v}||}$ and $\tilde{\psi}_{u,v} = \frac{\psi_{u,v}}{||\psi_{u,v}||}$ which constitute the (approximate) open-shell form of the exact wave function and the TDCIS wave function at $t = T/4$ for (a) $w = 1$ and (b) $w = 5$. All quantities in this figure are given in effective atomic units (see the Appendix).

Now, the approximation of the exact wave function in open-shell form allows a convenient comparison with the TDCIS wave function which can be exactly represented in open-shell form:

$$\Psi(x_1,x_2,t)_{\text{TDCIS}} = \psi_u(x_1,t)\psi_v(x_2,t) + \psi_v(x_1,t)\psi_u(x_2,t) \quad (21)$$

where

$$\psi_v(t) = \psi_0 \quad (22)$$

and

$$\psi_u(t) = \sum_i \tilde{\alpha}_i(t)\psi_i. \quad (23)$$

The two orbitals ϕ_u and ϕ_v and, respectively, ψ_u and ψ_v are only fixed up to a factor; i.e., a two-electron wave function in open-shell form is invariant under the transformation $\phi_u \to \phi_u/\alpha$, $\phi_v \to \alpha\phi_v$ where α is an arbitrary nonzero complex number. Therefore, we compare the TDCIS wave function with the exact wave function by consideration of the corresponding renormalized orbitals (see Fig. 3).

As can be observed in Fig. 3(a) for $w = 1$, i.e., for a confinement width for which the ionization probability is accurately reproduced by the TDCIS approach, within this open-shell approximation, both the exact and the TDCIS wave function are described by one orbital which is strongly localized in the potential well [ϕ_v (TDSE) and, respectively, ψ_v (TDCIS)] and one orbital which has overlap with the tunneling barrier describing a tunneling electron [ϕ_u (TDSE) and, respectively, ψ_u (TDCIS)]. Despite the fact that TDCIS reproduces accurately the ionization probability, deviations between these orbitals are observable. That is, within the exact treatment, the localized orbital ϕ_v (TDSE) is slightly shifted to the left with respect to the origin ($\langle x\rangle_{\phi_v} = \frac{\int |\phi_v|^2 x dx}{||\phi_v||^2} = -0.258$) whereas for the TDCIS approach the localized orbital (i.e., ψ_v) coincides with the Hartree-Fock ground-state orbital ψ_0 [see Eq. (22)] which is centered at the origin ($\langle x\rangle_{\psi_v} = \frac{\int |\psi_v|^2 x dx}{||\psi_v||^2} = 0$). However, both orbitals of both the TDCIS approach and the exact treatment (TDSE) are still mostly centered in close vicinity of the origin and differences are mostly observable for $x < 2$, i.e., within the potential well. Most importantly, within the tunneling barrier in vicinity of $x \gtrsim 2$, the density of the orbital that describes the tunneling electron mostly coincides with the density of the corresponding orbital obtained from the exact treatment. Hence, although there are deviations of the exact wave function to the TDCIS wave function within the confining potential, the TDCIS approach appears to provide an accurate description of the ionization process for this rather narrow confinement potential. However, for $w = 5$, the TDCIS approach is not able to reproduce accurately the ionization probability obtained by an exact treatment (TDSE). Still, within the open-shell approximation, the exact wave function is described by one orbital which is localized in the potential well [ϕ_v (TDSE)] and one orbital which has a significant overlap with the tunneling barrier [ϕ_u (TDSE)]. This indicates that, still, the dominant ionization process is also within the exact treatment a process where one electron resides in the potential well while the other is tunneling through the potential barrier. However, the localized orbital of the open-shell approximation of the exact wave function ϕ_v ($\langle x\rangle_{\phi_v} = 0.862$) is shifted towards the local minimum of the instantaneous potential at $x = 1.344$ whereas within the TDCIS approach the localized orbital is centered at the origin. Deviations are also observable between the orbitals describing the tunneling electron, i.e., ψ_u for the TDCIS approach and ϕ_u for the open-shell approximation of the exact wave function. In particular the orbital ϕ_u (TDSE) ($\langle x\rangle_{\phi_u} = 4.829$) is shifted towards the potential barrier maximum at $x = 6.385$ with respect to ψ_u (TDCIS) ($\langle x\rangle_{\psi_u} = 4.203$), resulting in a larger overlap of ϕ_u (TDSE) with the potential barrier. This indicates that the immobility of the localized electron within the TDCIS approach affects via the Coulomb interaction also the tunneling electron. That is, within the TDCIS approach, the tunneling electron seems to be less effectively pushed towards the tunneling barrier. This provides an explanation for the considerable differences between the ionization probability obtained by the TDCIS approach and the exact treatment. That is, in particular the underestimation of the ionization process by the TDCIS approach can be related to this circumstance (see Fig. 2). So far, only an open-shell approximation of the exact wave function has been considered, which approximates the full wave function fairly well (i.e., the overlap with the exact wave function is 0.967) but obviously there are still some deviations to the exact wave function. In the following section

we therefore provide more extensive insight into the light-induced multielectron dynamics from a different perspective by considering the complete wave function obtained from the exact treatment.

B. Field-induced multielectron motion

Due to the fact that the level spacing of the confinement ΔE is much larger than the frequency of the light field, i.e., $\Delta E \geqslant 0.48 \gg \omega = 2\pi \times 0.001$, the low-frequency field considered here can induce a quasiadiabatic electron motion leading to a time-dependent shift of the electronic center of-mass. Within the harmonic approximation of the confining potential and within the dipole approximation, this motion of the electronic center of mass can be related to a shift of the confining potential minimum:

$$\Delta x = \frac{E(t)w^2}{2V_0}. \tag{24}$$

This effect causes a shift of the density with respect to the origin (see Fig. 6). Noteworthy, this shift of the potential minimum results in the motion of both electrons, which becomes noticeable in the open-shell approximation [see Eq. (18)] by the fact that the orbital ϕ_v, which describes a localized electron, is not centered at the origin but is rather shifted towards the local minimum of the instantaneous potential (see Fig. 3). The regime of large deviations of the ionization probability obtained by TDCIS and exact treatment coincides with the regime where Δx is on the order of the Bohr radius or larger, i.e., $\Delta x \gtrsim 1 \mathrel{\widehat{=}} w \gtrsim 4.5$. This supports the explanation for the large deviations between the ionization probability obtained by TDCIS and exact treatment as given in the previous section. That is, within the TDCIS approach, the tunneling electron is less effectively pushed towards the tunneling barrier due to the immobility of the localized electron. However, since the considered confining potential well is not a pure harmonic potential also excitations of the relative motion are possible [18]. This allows for correlated electron dynamics. In order to get insight into this light-induced correlation dynamics, we consider electronic correlations which become noticeable by the circumstance that the electronic wave function cannot be represented by a single Slater determinant. Therefore, we determine the degree of correlation of the two-electron wave function by employing the measure of correlations K as defined in [32]:

$$K = \left(\sum_i n_i^2\right)^{-1} \tag{25}$$

where n_i denote the occupation numbers of the natural orbitals, i.e., the eigenvalues of the first-order density matrix [33]. Thereby, K can be interpreted as the "number" of Slater determinants which are effectively necessary to represent the wave function (see [32]). Since every fully uncorrelated singlet two-electron wave function is a Slater determinant with a doubly occupied spatial orbital, the absence of correlations is characterized by a measure of correlations $K = 1$. Thus, electronic correlations manifest themselves by a value of K larger than 1 (note that $n_i > 0$ and $\sum_i n_i = 1$ (see [33] and [29]). In order to determine K numerically, we obtain the occupation numbers of the natural orbitals by diagonalization of the first-order density matrix [29] represented on a spatial grid.

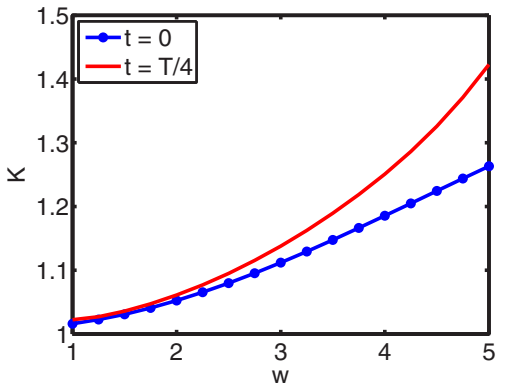

FIG. 4. (Color online) The degree of correlations K as defined in Eq. (25) in dependence of the width of the confinement w for the singlet ground state (blue curve with dots) and at the time when the electric field of the laser is strongest ($t = T/4$) (red curve). All quantities in this figure are given in effective atomic units (see the Appendix). Since the relative strength of the Coulomb interaction increases with increasing width of the confining potential, the amount of correlations present in the ground state increases correspondingly (blue curve with dots). While for narrow confinements ($w \approx 1$) the amount of correlations remains constant, for broad confinement potentials, in the presence of the light field, the amount of correlations is significantly increased in comparison to the ground state.

In Fig. 4, K is shown in dependence on the width w of the confining potential for two situations, i.e., for the singlet ground state (blue curve with dots) and for the two-electron wave function at $t = T/4$ (red curve). As can be seen in Fig. 4, for narrow confinements ($w \approx 1$) the measure of correlations K for the singlet ground state is nearly 1, indicating an accurate description by the Hartree-Fock determinant (for $w = 1$ one finds indeed that mostly only one natural orbital is populated in the ground state with an occupation of 0.992). However, K increases monotonically with the confining potential width. This is related to a feature well known for the harmonic confinement potential, namely, that the confinement energy and the Coulomb interaction scale differently with respect to the characteristic confinement length l_0. That is, whereas the confinement energy scales as $\frac{1}{l_0^2}$, the Coulomb interaction is proportional to $\frac{1}{l_0}$. Hence, the relative strength of the Coulomb interaction increases monotonically with the width of the confinement potential, leading to a correspondingly increasing population of more than one natural orbital (see Fig. 5). For $w = 5$, one finds that a second natural orbital is significantly populated with an occupation of 0.107 so that here a multideterminant treatment is already necessary to represent the ground state accurately (note that the overlap with the Slater determinant with maximum overlap with the exact wave function is given by $\sqrt{n_1} = 0.9398$ where n_1 is the occupation number of the most occupied natural orbital (see [29])).

However, if one considers the two-electron wave function at $t = T/4$, one observes a significant enhancement of correlations with respect to the ground-state correlations. For instance for $w = 5$, the occupation of the second most occupied natural

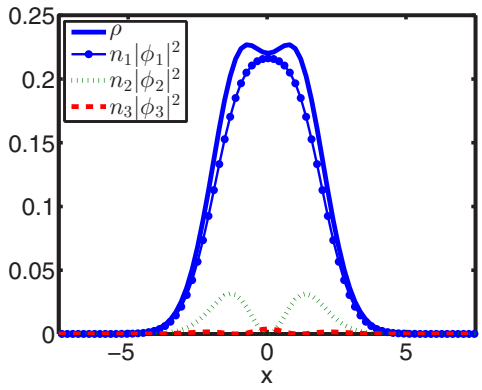

FIG. 5. (Color online) The probability density ρ of the singlet ground state and the densities of the first three most occupied natural orbitals ϕ_1,ϕ_2 and ϕ_3 weighted by their occupation numbers (n_1, n_2, and n_3) for a relatively wide confining potential ($w = 5$). All quantities in this figure are given in effective atomic units (see the Appendix). Due to a strong Coulomb interaction with respect to the confinement energy, more than one natural orbital is significantly occupied in the ground state.

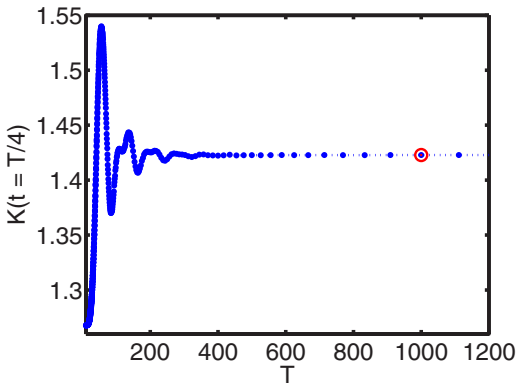

FIG. 7. (Color online) The degree of correlations K [see Eq. (25)] at $t = T/4$ for $w = 5$. All quantities in this figure are given in effective atomic units (see the Appendix). Nonadiabatic excitations within the potential well manifest themselves by a frequency dependence of K for $T < 400$, i.e., for frequencies larger than $2\pi \times 0.0025$. Thus, for the considered laser frequency ($2\pi \times 0.001$, big red marker) nonadiabatic effects appear to be irrelevant.

orbital increases from 0.107 to even 0.142 in the presence of the light field and furthermore also a third natural orbital becomes noticeably populated with an occupation of $\approx$0.028 whereas its ground-state occupation is only 0.009 (see Fig. 6). Note that the occupation of a third natural orbital is not included in the open-shell approximation [see Eq. (18)] and thus represents a deviation between the TDCIS wave function and exact wave function that adds to those discussed in the previous section.

Since the degree of correlations at $t = T/4$ is independent of the laser frequency for frequencies smaller than $2\pi \times 0.0025$ (see Fig. 7), nonadiabatic excitations within the potential well are apparently not the reason for the enhancement of K (the considered laser frequency is $2\pi \times 0.001$). Since the most occupied natural orbitals are localized within the well of the instantaneous potential, this effect can be attributed to a quasiadiabatic rearrangement of the still trapped electrons within this strongly deformed potential well. The enhancement of the degree of correlations indicates here an effective broadening of the potential well by the light field which results in an enhanced effective strength of the Coulomb interaction between the still trapped electrons. According to Eq. (24) and, respectively, Eq. (9), an increase of the width of the confining potential is accompanied by both an increased light-induced shift of the potential minimum and, as indicated by a decreasing critical field strength E_{crit}, an increased light-induced distortion of the potential well. Apparently, as the result of this effective weakening of the confining potential, both the light-induced collective and the correlated electron motion increase for wide confinements.

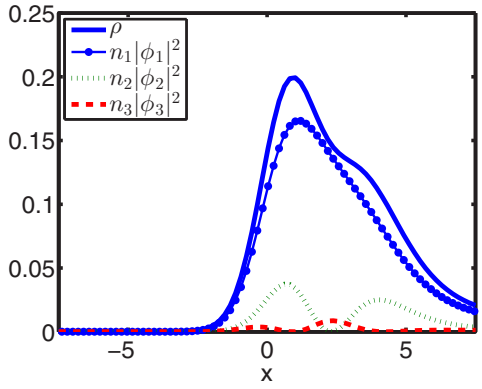

FIG. 6. (Color online) The probability density ρ of the two-electron state at the time when the electric field of the laser is strongest ($t = T/4$) and the densities of the first three most occupied natural orbitals ϕ_1,ϕ_2, and ϕ_3 weighted by their occupation numbers for a relative wide confining potential ($w = 5$). All quantities in this figure are given in effective atomic units (see the Appendix). In comparison to the ground state (see Fig. 5), the occupation of the second and the third most occupied natural orbital is increased.

IV. CONCLUSIONS

To conclude, we demonstrated that for an accurate description of the tunneling ionization process a multielectron description is the more important the wider the confining potential. By analysis of the exact wave function, we show that a multielectron description is not only necessary due to ground-state correlations but also due to a collective and correlated multielectron motion resulting from the deformation of the confining potential well by the light field.

ACKNOWLEDGMENTS

The authors are grateful to Robin Santra for many instructive discussions. This work was funded by the Deutsche Forschungsgemeinschaft under both the grant SFB 925 and the excellence cluster "The Hamburg Centre for Ultrafast Imaging—Structure, Dynamics, and Control of Matter on the Atomic Scale".

APPENDIX

Throughout this paper, we employ effective atomic units (see [20]). That is, energies are given in effective Hartree $\tilde{E}_H$,

$$\tilde{E}_H = \frac{m^* e^4}{(4\pi\epsilon_0\epsilon_r\hbar)^2}; \tag{A1}$$

length is given in units of the effective Bohr radius $\tilde{a}_0$,

$$\tilde{a}_0 = \frac{4\pi\epsilon_0\epsilon_r\hbar^2}{m^* e^2}; \tag{A2}$$

time is given in units of $\tilde{t}_0$,

$$\tilde{t}_0 = \frac{\hbar}{\tilde{E}_H}; \tag{A3}$$

velocity is given in units of $\tilde{v}_0$,

$$\tilde{v}_0 = \frac{\tilde{a}_0\tilde{E}_H}{\hbar}; \tag{A4}$$

electric field strength is given in units of $\tilde{\mathcal{E}}_0$,

$$\tilde{\mathcal{E}}_0 = \frac{\tilde{E}_H}{e\tilde{a}_0}; \tag{A5}$$

and intensity is given in units of $\tilde{I}_0$,

$$\tilde{I}_0 = \tilde{\mathcal{E}}_0^2, \tag{A6}$$

where m_e^* denotes the effective electron mass, ϵ_0 is the electric constant, ϵ_r is the dielectric constant, $\hbar$ is the Planck constant, and e is the electron charge.

For atoms and molecules, the effective electron mass m^* coincides with the electron mass and the dielectric constant ϵ_r is 1. Hence, for atoms and molecules, the chosen unit system coincides with the well-known atomic units. However, for instance for GaAs quantum dots, the effective electron mass m^* is only 0.067 times the electron mass and the dielectric constant ϵ_r is 12.4 so that, for instance, an effective Hartree corresponds to 11.86 meV and an intensity $1.0 \times \tilde{I}_0$ corresponds to only 1.95×10^5 W/cm^2.

[1] K. C. Kulander, Time-dependent theory of multiphoton ionization of xenon, Phys. Rev. A **38**, 778 (1988).

[2] K. Kulander and T. Rescigno, Effective potentials for time-dependent calculations of multiphoton processes in atoms, Comput. Phys. Commun. **63**, 523 (1991).

[3] K. C. Kulander and B. W. Shore, Calculations of Multiple-Harmonic Conversion of 1064-nm Radiation in Xe, Phys. Rev. Lett. **62**, 524 (1989).

[4] N. Rohringer, A. Gordon, and R. Santra, Configuration-interaction-based time-dependent orbital approach for *ab initio* treatment of electronic dynamics in a strong optical laser field, Phys. Rev. A **74**, 043420 (2006).

[5] S. Pabst and R. Santra, Strong-field Many-Body Physics and the Giant Enhancement in the High-Harmonic Spectrum of Xenon, Phys. Rev. Lett. **111**, 233005 (2013).

[6] J. C. Tremblay, T. Klamroth, and P. Saalfrank, Time-dependent configuration-interaction calculations of laser-driven dynamics in presence of dissipation, J. Chem. Phys. **129**, 084302 (2008).

[7] K. Raghavachari and J. B. Anderson, Electron correlation effects in molecules, J. Phys. Chem. **100**, 12960 (1996).

[8] D. Pfannkuche, V. Gudmundsson, and P. A. Maksym, Comparison of a Hartree, a Hartree-Fock, and an exact treatment of quantum-dot helium, Phys. Rev. B **47**, 2244 (1993).

[9] D. Pfannkuche, R. R. Gerhardts, P. A. Maksym, and V. Gudmundsson, Theory of quantum dot helium, Physica B **189**, 6 (1993).

[10] B. Szafran, J. Adamowski, and S. Bednarek, Electron-electron correlation in quantum dots, Physica E **5**, 185 (1999).

[11] T. M. Henderson, K. Runge, and R. J. Bartlett, Electron correlation in artificial atoms, Chem. Phys. Lett. **337**, 138 (2001).

[12] C. Bruder and H. Schoeller, Charging Effects in Ultrasmall Quantum Dots in the Presence of Time-Varying Fields, Phys. Rev. Lett. **72**, 1076 (1994).

[13] J. Splettstoesser, M. Governale, J. König, and M. Büttiker, Charge and spin dynamics in interacting quantum dots, Phys. Rev. B **81**, 165318 (2010).

[14] D. Sokolovski, Resonance tunneling in a periodic time-dependent external field, Phys. Rev. B **37**, 4201 (1988).

[15] T. H. Oosterkamp, L. P. Kouwenhoven, A. E. A. Koolen, N. C. van der Vaart, and C. J. P. M. Harmans, Photon Sidebands of the Ground State and First Excited State of a Quantum Dot, Phys. Rev. Lett. **78**, 1536 (1997).

[16] K. Shibata, A. Umeno, K. M. Cha, and K. Hirakawa, Photon-Assisted Tunneling Through Self-Assembled InAs Quantum Dots in the Terahertz Frequency Range, Phys. Rev. Lett. **109**, 077401 (2012).

[17] F. Gallego-Marcos, R. Sánchez, and G. Platero, Photon assisted long-range tunneling, J. Appl. Phys. **117**, 112808 (2015).

[18] L. Jacak, P. Hawrylak, and A. Wojs, *Quantum Dots* (Springer, New York, 1998).

[19] J. Adamowski, M. Sobkowicz, B. Szafran, and S. Bednarek, Electron pair in a Gaussian confining potential, Phys. Rev. B **62**, 4234 (2000).

[20] Y. Sajeev and N. Moiseyev, Theory of autoionization and photoionization in two-electron spherical quantum dots, Phys. Rev. B **78**, 075316 (2008).

[21] W. Häusler and B. Kramer, Interacting electrons in a one-dimensional quantum dot, Phys. Rev. B **47**, 16353 (1993).

[22] O. Ciftja and M. G. Faruk, Two interacting electrons in a one-dimensional parabolic quantum dot: Exact numerical diagonalization, J. Phys.: Condens. Matter **18**, 2623 (2006).

[23] M. Feit, J. A. Fleck, Jr., and A. Steiger, Solution of the Schrödinger equation by a spectral method, J. Comput. Phys. **47**, 412 (1982).

[24] O. Shemer, D. Brisker, and N. Moiseyev, Optimal reflection-free complex absorbing potentials for quantum propagation of wave packets, Phys. Rev. A **71**, 032716 (2005).

[25] L. Greenman, P. J. Ho, S. Pabst, E. Kamarchik, D. A. Mazziotti, and R. Santra, Implementation of the time-dependent configuration-interaction singles method for atomic strong-field processes, Phys. Rev. A **82**, 023406 (2010).

[26] L. V. Keldysh, Ionization in the field of a strong electromagnetic wave, Sov. Phys. JETP **20**, 1307 (1965).

[27] T. J. Park and J. C. Light, Unitary quantum time evolution by iterative Lanczos reduction, J. Chem. Phys. **85**, 5870 (1986).

[28] U. Merkt, J. Huser, and M. Wagner, Energy spectra of two electrons in a harmonic quantum dot, Phys. Rev. B **43**, 7320 (1991).

[29] P.-O. Löwdin and H. Shull, Natural orbitals in the quantum theory of two-electron systems, Phys. Rev. **101**, 1730 (1956).

[30] K. J. H. Giesbertz, Ph.D. thesis, Free University Amsterdam, 2010.

[31] M. Brics and D. Bauer, Time-dependent renormalized natural orbital theory applied to the two-electron spin-singlet case: Ground state, linear response, and autoionization, Phys. Rev. A **88**, 052514 (2013).

[32] S. L. Haan, R. Grobe, and J. H. Eberly, Numerical study of autoionizing states in completely correlated two-electron systems, Phys. Rev. A **50**, 378 (1994).

[33] P.-O. Löwdin, Quantum theory of cohesive properties of solids, Adv. Phys. **5**, 1 (1956).